CO and CH_4 total oxidation over manganese oxide supported on ZrO_2, TiO_2, TiO_2–Al_2O_3 and SiO_2–Al_2O_3 catalysts

Mohamed I. Zaki,[a]* Muhammad A. Hasan,[a] Lata Pasupulety,[a] Nasr E. Fouad[b] and Helmut Knözinger[b]

[a] *Chemistry Department, Faculty of Science, Kuwait University, P.O. Box 5969, Safat 13060, Kuwait. Fax: +0965 484 6946; E-mail: Zaki@kuc01.kuniv.edu.kw.*

[b] *Institut für Physikalische Chemie, Universität München, Butenandtstrasse 5-13 (Haus E), 81377 München, Germany*

Received* (*in Montpellier, France*) *14th September 1999, Accepted 12th October 1999

Zirconia, titania, titania–alumina and silica–alumina supported and unsupported MnO_x catalysts were prepared and characterized by X-ray diffractometry and photoelectron spectroscopy, infrared spectroscopy and nitrogen sorptometry. Their catalytic activities were tested towards total oxidation of carbon monoxide and methane. The results show the unsupported MnO_x (exposed on an α-Mn_2O_3 bulk structure) to catalyze CO oxidation at $\leqslant 250\,^{\circ}C$ and CH_4 oxidation at $\geqslant 250\,^{\circ}C$, and to remain chemically and structurally stable. The CO oxidation activity of MnO_x is improved when dispersed on zirconia, whereas its CH_4 oxidation activity is improved on silica–alumina. These results may help in concluding that (*i*) CO oxidation is not the rate determining step of the oxidation of CH_4, (*ii*) availability of strong acid sites (as those exposed on silica–alumina) is important for CH_4 oxidation and (*iii*) the difference in the catalytic activity towards the oxidation of CO and CH_4 resides in the need for different catalytic functions for each reaction, which are, therefore, not related in terms of kinetic control.

Natural gas-fueled turbines are expected to provide a significant portion of the growing world demand for electric power generation.[1] The propellant gas is generated by catalytic or flame combustion of the natural gas, which is constituted essentially of CH_4. The catalytic combustion technology is advantageous for lower emission levels of NO_x species in the exhaust.[1,2] However, it is challenged by the demand for catalysts of extreme thermal and chemical stability, and sustained activity in the highly oxidizing, high temperature (up to 1300–1500 °C) combustion environment.[1]

The most intrinsically active catalysts for methane combustion are the noble metals,[1] particularly platinum and palladium. However, noble metals are susceptible to sintering, and form volatile oxides under the combustion conditions.[1] Promising alternative catalysts are metal oxide composites, particularly those assuming perovskite[1–4] and spinel[5] structures, as well as transition metal oxides dispersed on high surface area metal oxide supports of stable phase composition at high temperatures,[1,6,7] *viz.* cordierite ($2MgO \cdot 5SiO_2 \cdot 2Al_2O_3$), mullite ($3Al_2O_3 \cdot 2SiO_2$) and aluminium titanate. The oxidation activity of these metal oxide catalysts has been found[2–4] to optimize in an electron-mobile environment established by d-d electron exchange interactions involving metal atoms of different oxidation states.

There is a general consensus[2–4,8–10] on the following activity and mechanistic aspects: (*i*) CO is the primary oxidation product of CH_4, and CO_2 is generated subsequently by oxidation of CO, (*ii*) on reduced surfaces, both CH_4 conversion and CO selectivity are high, (*iii*) on oxidized surfaces, the CH_4 conversion and CO selectivity are low, (*iv*) the rate determining step is the recombination of surface carbon and oxygen atoms to form CO ($C_s + O_s \rightarrow CO_s$), (*v*) at high temperatures, the CH_4 oxidation activity is inversely proportional to the $M–O_{cat}$ bond energy (Mars–van Krevelen-type mechanism) and (*vi*) at low temperatures, the activity is directly proportional to the covalency of $M–O_{ads}$ bonds (Eley–Rideal or Langmuir–Hinshelwood-type mechanism). *In situ* IR investigations[5,11] have provided sufficient evidence in support for the above mechanistic aspects.

The present investigation was designed to compare the total oxidation (combustion) activity of supported Mn_2O_3 catalyst samples towards CH_4 and CO in an oxygen-rich atmosphere. The supports adopted were high surface area ZrO_2, TiO_2, TiO_2–Al_2O_3 and SiO_2–Al_2O_3. The thrust behind the investigation are the following considerations: (*i*) Mn_2O_3 based catalysts are amongst the most active catalysts for CO and hydrocarbon oxidation;[2,9–12] Mn-containing perovskites have been found to assure a comparable oxidation activity to that of Pt- and Pd-based catalysts,[13,14] (*ii*) Mn oxides assume a wide range of polymeric, simple and mixed compositions with Mn atoms in different oxidation states, for example Mn_5O_8 ($Mn^{II}_2Mn^{IV}_3O_8$) and Mn_3O_4 ($Mn^{II}Mn^{III}_3O_4$),[15] which can, according to Zener,[16] establish the necessary electron-mobile environment for optimal surface redox catalysts, (*iii*) the test supports include materials known for their high thermal stability and strong metal-support interactions,[17] (*iv*) the comparative reactivity of a given catalyst towards the oxidation of CH_4 and CO should help in a greater understanding of the catalytic combustion pathways, for the latter molecule is considered the primary oxidation product of the former.[5]

Experimental

Materials

Supported manganese oxide catalysts (10 wt.% Mn_2O_3) were obtained by 700 °C calcination for 3 h of support materials impregnated with an aqueous solution of 99% pure BDH $Mn(NO_3)_2 \cdot 4H_2O$. The support materials were Degussa titania P25 (Ti; 50 $m^2\ g^{-1}$) and 3 wt.% titania–alumina (TiAl; 139 $m^2\ g^{-1}$), MEL zirconia (Zr; 41 $m^2\ g^{-1}$), and Akzo 5 wt.% silica–alumina (SiAl; 411 $m^2\ g^{-1}$); these were used as supplied. The impregnation was carried out by 30 min magnetic stirring of a suspension of the appropriate amount of the

support particles in the impregnating solution (~10 mL of solution per 1 g of the support) at RT, evaporating the excess solvent at 100 °C for 48 h, grinding of the solid residue, and further drying at 100 °C for 24 h. Neither the impregnated supports, nor the final supported catalysts (denoted Mn/Ti, Mn/Zr, Mn/TiAl, Mn/SiAl) were subjected to solid state analysis for the actual loading of Mn_2O_3. An appropriate analytical technique (*e.g.*, XRF) was out of reach. For comparison purposes, unsupported Mn_2O_3 catalyst (denoted Mn) was prepared *via* similar 700 °C calcination for 3 h of the parent nitrate compound.

The reactants were 99.995% pure CH_4 and O_2 (Linde, Germany) and 99.999% pure CO and O_2 (KOAC, Kuwait). Helium gas, which was used as a carrier in CH_4 experiments, and as a diluent in CO experiments, was 99.999% pure (Linde and KOAC).

Catalyst characterization

X-ray powder diffractometry (XRD) was carried out at ambient temperature, on a Siemens D5000 diffractometer (Germany) using Ni-filtered CuKα radiation (λ = 1.5418 Å, 40 kV, 30 mA) in the 2θ range of 10–80° with a divergence slit of 1°. The diffractograms, recorded stepwise (step size = 0.02°, step time = 15 s), were acquired and handled with an on-line microcomputer. For phase identification purposes, automatic JCPDS library search (standard SEARCH software) and match (standard DIFFRAC AT software) were performed.

Infrared (IR) spectra were taken from KBr-supported test materials (≤1 wt.%) over the frequency range of 4000–400 cm^{-1} and at a resolution of 4 cm^{-1}, using a model 2000 Perkin–Elmer FT spectrometer (UK). An on-line data station facilitated spectra acquisition and manipulation.

Surface area and chemical composition were determined using N_2 gas sorptometry and X-ray photoelectron spectroscopy (XPS), respectively. The gas sorptometry was measured at liquid nitrogen temperature (−195 °C), using an automatic ASAP 2010 Micromeritics sorptometer (USA), equipped with a computing facility capable of running a BET analysis of the adsorption data. The test materials were pre-outgassed at 100 °C for 12 h, and the adsorptive gas was 99.999% pure N_2 (KOAC) XPS spectra were recorded on a model VG Scientific 200 (UK) spectrometer using AlKα radiation (1486.6 eV) operating at 300 W, 13 kV and 33 mA. The spectra acquisition and handling were conducted by means of an on-line ECLIPSE data system (UK). The surface atomic percentages of elements encountered was calculated from the peak areas (in counts eV s^{-1}) with integral subtraction of the background.

Catalytic activity tests

Catalytic activity towards CH_4 oxidation was tested by means of a flow assembly equipped with a 9 mm i.d. microreactor, by feeding a gas mixture of CH_4 (5%), O_2 (25%) and He (70%) at a total flow rate of 100 mL min^{-1} through thin catalyst flakes (250–300 mg) loaded on an integral quartz frit. Prior to reaction, the catalyst was activated by flushing with 100 mL min^{-1} of O_2 at 400 °C for 30 min. The gases were analyzed by means of a model 3400 Varian gas chromatograph equipped with a 25 m long Chrompack PoraPLOT Q micro-column, an FID detector and a model 4290 Varian integrator for data processing.

On the other hand, catalytic activity towards CO oxidation was tested using a gas circulating assembly (analogous to that designed in the past by Schwab *et al.*[18]), by charging a 20 mm i.d. tubular reactor with a gas mixture of CO and O_2 (in a 1 : 3 mass ratio) at a total pressure of 300 torr (1 torr = 133.3 Pa). Thin flakes of the catalyst (250–300 mg), loaded on an integral quartz frit, were pre-activated by *in situ* heating in 4 successive charges of 200 torr of O_2 at 200 °C for 15 min per charge. GC quantitative analysis of 50 μL gas samples withdrawn from the reaction atmosphere by means of a Hamilton gas syringe was carried out using a model CP-9001 Chrompack chromatograph (The Netherlands), equipped with a TCD detector, a PoraPack Q column and a MOSAIC software for data acquisition and processing.

It is important to note that each reaction temperature applied (25–500 °C) was maintained for a constant period of time (10 min) prior to gas sampling (3 samples) for analysis. Neither the constant flow rate (case of CH_4 oxidation) nor the gas circulating assembly (case of CO oxidation) adopted facilitated making a precise assessment of the diffusion control over the reaction kinetics.

Results and discussion

Catalyst characteristics

Bulk crystalline structure. Fig. 1 compares X-ray powder diffractograms obtained for the unsupported (Mn) and supported catalysts. Results obtained therefrom are summarized in Table 1. The crystalline bulk structure of Mn is shown to be constituted of large crystallites (average size = 40 nm) of Bixbyite-like α-Mn_2O_3 (JCPDS 41-1442). When supported, MnO_x species are shown to crystallize also into the same modification of α-Mn_2O_3; however smaller crystallites are formed. On titania–containing supports, *viz.* Ti (=anatase TiO_2; JCPDS 21-1272) and TiAl (noncrystalline), the average crystallite size is reduced to 30 and 19 nm, respectively. On Zr (=monoclinic ZrO_2; JCPDS 37-1484), the average crystallite size of α-Mn_2O_3 is reduced further to 15 nm. The maximal reduction in the crystallite size is that (8 nm) shown to occur on SiAl (noncrystalline). In all supported Mn_2O_3 catalyst

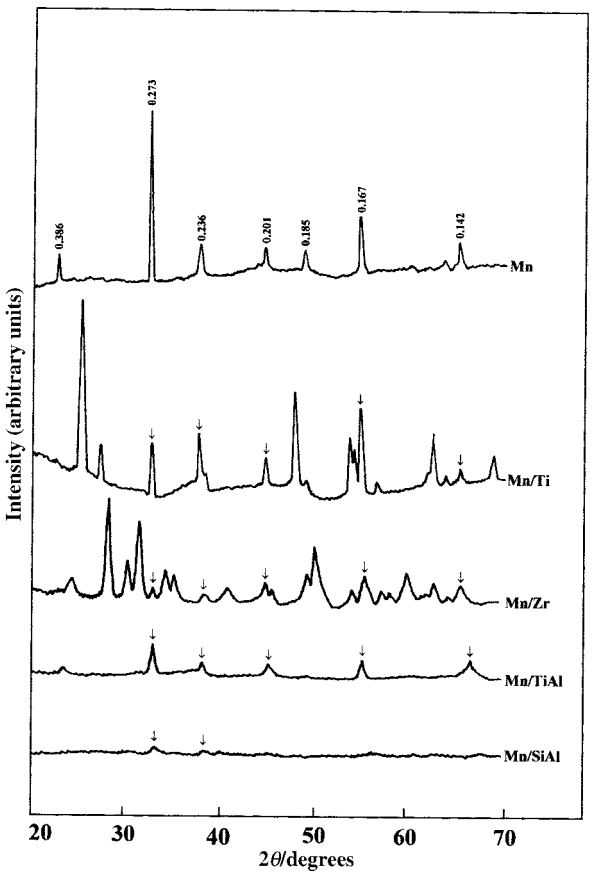

Fig. 1 X-ray powder diffractograms for the unsupported (Mn) and supported catalysts. Diffraction peaks monitored in the diffractogram of Mn are marked by the interplaner d-spacing values (in nm), and further indicated in the diffractograms of the supported catalysts by arrows (↓).

Table 1 Bulk and surface characteristics of the catalysts

Catalyst	Bulk MnO_x		Surface area[c] /$m^2\ g^{-1}$	Surface chemical composition[d]									
	Crystalline phase[a]	Crystallite size[b]/nm		Al(2p)		Zr(3p3/2)		Ti(2p3/2)		O(1s)		Mn(2p3/2)	
				eV	%	eV	%	eV	%	eV	%	eV	%
Mn	α-Mn_2O_3(s)	40	7	—	—	—	—	—	—	529.2	60.3	641.1	39.7
Mn/Zr	α-Mn_2O_3(t)	15	33(41)	—	—	334.0	26.5	—	—	529.1		641.5	5.6
										531.4	67.9		
Mn/Ti	α-Mn_2O_3(m)	30	13(50)	—	—	—	—	457.3	44.9	529.5		640.9	3.2
										531.5	51.9		
Mn/TiAl	α-Mn_2O_3(t)	19	113(139)	74.0	52.9	—	—	458.1	1.1	529.9		640.7	4.7
										531.0	41.3		
Mn/SiAl	α-Mn_2O_3(h)	8	268(411)	75.0	28.2	—	—	—	—	529.0		640.5	8.9
										531.4	62.9		

[a] s = sole; m = minor; t = trace; h = hardly detectable. [b] Average crystallite size approximated by applying the X-ray line broadening technique.[19] [c] Parenthesized value is for the unloaded support. [d] Si was not detectable on Mn/SiAl; calculation of atomic ratios excluded minute amounts of C(1s) impurity atoms observed at 284.2 eV.

samples, however, no sign of formation of mixed crystalline phases of MnO_x and the support is observed (Fig. 1).

The above XRD results are supported by IR spectra of the catalysts (Fig. 2). νMn–O absorptions exhibited by Mn at 670, 602, 578 and 528 cm^{-1} are very close to those (at 666, 599, 574 and 523 cm^{-1}) reported previously[20] for Mn–O lattice vibrations of mineral-grade α-Mn_2O_3. Despite rather strong IR absorptions exhibited by the support materials over the frequency range of interest (Fig. 2), νMn–O absorptions due to α-Mn_2O_3 can be discerned in the spectra of Mn/Ti (at 578 cm^{-1}), Mn/TiAl (at 579 cm^{-1}), Mn/Zr (at 564 cm^{-1}) and Mn/SiAl (at 578 cm^{-1}). The spectra of Mn_2O_3-loaded supports are almost identical to those of unloaded supports (Fig. 2), except for SiAl. Mn/SiAl exhibits two unique features: (*i*) a newly emerging broad shoulder in the range 780–880 cm^{-1}, and (*ii*) suppression of the absorption at 1072 cm^{-1}. The latter feature may imply the breaking of Si–O–Al bridge bonds,[21] whereas the former feature may arise from formation of a mixed $MnAlO_x$ species. Both features are likely to be interrelated. The failure of XRD to detect mixed crystalline phases of $MnAlO_x$ or $MnSiO_x$ may imply that the IR-detected formation of $MnAlO_x$ species is confined to too small crystallites to be XRD-detected.

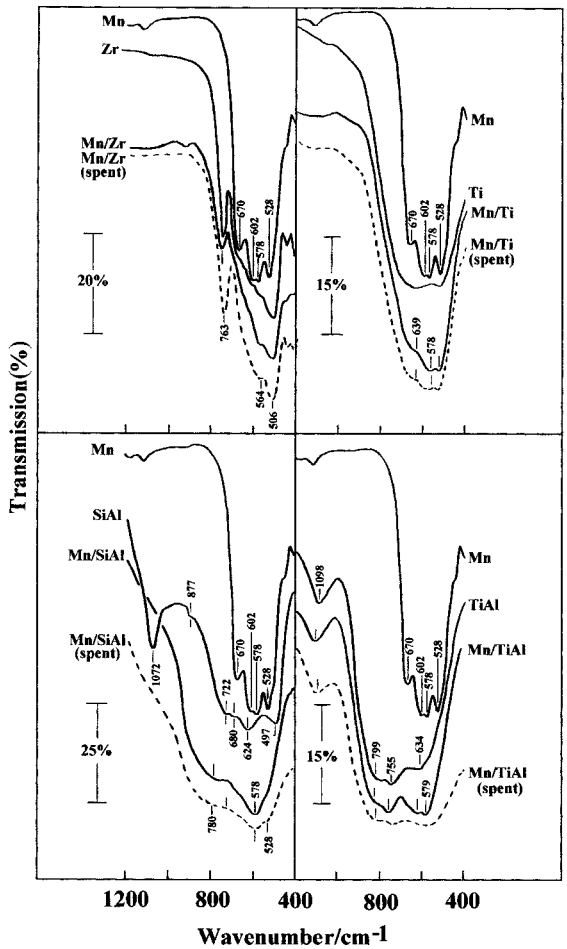

Fig. 2 IR spectra for fresh (——) and spent (– – –) catalysts. Spectra of unloaded supports are included for comparison purposes.

The above results indicate that the test supports have surfaces of various dispersing capacities towards Mn_2O_3 particles, namely Ti ⩽ TiAl < Zr ≪ SiAl. According to Che and Bonneviot,[22] dispersion of supported catalytic species is determined by any, or all, of the following parameters: (*i*) adsorption selectivity of support particles when suspended in the impregnating solution of catalyst ionic species, (*ii*) solid/solid wettability at catalyst/support interfaces in impregnated supports, and (*iii*) heat-enhanced chemical reactivity at the catalyst/support interfaces. The fact that surfaces of the test supports would acquire a net positive charge (pH_{zpc} = 5–6)[23] in the acidic medium (pH = 4–5) of the impregnating solution of $Mn(NO_3)_2$, may suppress their adsorptive affinity towards positively charged Mn^{2+} ions in solution.[23–25] Thus, the first parameter may be rendered unlikely to play a determining role towards the dispersing capacity of the present supports. On the other hand, IR-observed formation of mixed $MnAlO_x$ species in Mn/SiAl may highlight the importance of the last parameter (heat-enhanced chemical reactivity). It is worth mentioning, however, that one cannot exclude the large differences in the support surface areas from playing a role in determining the support dispersion capacity.

Surface area and chemical composition. Table 1 shows the unsupported Mn catalyst to expose surfaces of poor specific area (7 $m^2\ g^{-1}$) and a chemical composition constituted solely of Mn^{3+} and O^{2-} lattice sites. The O/Mn atomic ratio (=1.52) is almost identical to that of the stoichiometry of Mn_2O_3. Table 1 shows, moreover, that loading of Mn_2O_3 species results in varied losses of the support surface area. The loss is shown to maximize on Mn/Ti (50 → 13 $m^2\ g^{-1}$; 74%), and to minimize on both Mn/TiAl (139 → 113 $m^2\ g^{-1}$; 19%) and Mn/Zr (41 → 33 $m^2\ g^{-1}$; 20%). These results suggest that the loss of surface area of the loaded supports may be attributed to a change of surface chemistry of the supports (*e.g.*, formation of $MnAlO_x$ species on Mn/SiAl) and/or pore blockage by Mn_2O_3 particles (presumably in the case of Mn/Ti). It

is noteworthy that addition of a small amount (3 wt.%) of titania to alumina renders the supporting surface more resistant to area losses caused by loading MnO_x species.

The surface composition of supported Mn_2O_3 catalyst samples is shown (Table 1) to be constituted of lattice elements of both Mn_2O_3 and the support, as well as OH groups [O(1s) electron binding energy (BE) = 531.0–531.5 eV]. Corresponding IR spectra displayed consistently medium-to-strong bands due to νOH vibrations of surface OH groups at 3856, 3754 (isolated OHs) and 3444 cm^{-1} (associated OH's) for Mn/SiAl; 3774 (isolated) and 3433 cm^{-1} (associated) for Mn/Zr; 3794 (isolated) and 3450 cm^{-1} (associated) for Mn/Ti; and 3774 (isolated) and 3450 cm^{-1} (associated) for Mn/TiAl. In addition, weak bands due to δOH vibrations of surface H_2O molecules were monitored at 1637–1629 cm^{-1} for supported Mn_2O_3 catalyst samples. Relatively speaking, the strongest bands of νOH and δOH were observed for Mn/SiAl, and the weakest bands were monitored for Mn/Ti.

Thus, XPS results (Table 1) may lead to the following conclusions regarding supported Mn_2O_3 catalyst samples. First, all of the test samples contain two different surface oxygen-containing species, *viz.* lattice O^{2-} sites [O(1s) BE = 529.0–529.9 eV][26] and OH groups (BE = 531.0–531.5 eV). The respective O(1s) binding energy values may imply that the lattice O^{2-} sites are relatively more basic in character on Mn/SiAl and Mn/Zr than on the other two supported catalyst samples. Second, the Mn(2p3/2) electron binding energy assumes higher and lower values than that shown by Mn^{3+} sites exposed on the unsupported Mn_2O_3 catalyst (BE = 641.1 eV), which may indicate coexistence of supported Mn sites in higher and lower oxidation states than 3+.[26] This may be particularly true for Mn/Zr [Mn(2p3/2) BE = 641.5 eV] and Mn/SiAl (BE = 640.9 eV), where occurrence of $Mn^{\geqslant 3+}$ and $Mn^{\leqslant 3+}$ sites may, respectively, be expected.[26] Third, the atomic ratio of Mn to total metal sites is higher on Mn/SiAl (0.32) than on Mn/Zr (0.21), and much higher than on Mn/Ti (0.07) and Mn/TiAl (0.09). This may correlate with the XRD-anticipated higher dispersion (smaller crystallite size) of Mn_2O_3 on SiAl and Zr than on the other two supports. Fourth, Si sites are not detectable on surfaces of Mn/SiAl. This result, when correlated with the IR-observed elimination of Si–O–Al bridge bonds of the loaded support (Fig. 2), may be considered compatible with the high dispersion of Mn_2O_3 on SiAl.

Stability under working conditions. A prime consideration for the appropriateness of promising combustion catalysts is their ability to withstand, chemically and structurally, the high temperature oxidative conditions of combustion.[1] Therefore, the present supported and unsupported Mn_2O_3 catalysts were subjected to XRD and IR analyses, following utilization in catalytic tests towards oxidation of CO and CH_4. Results obtained for the spent catalysts were almost identical to those exhibited by the fresh catalysts (unused). For example, IR spectra of spent supported catalyst samples are compared with those taken of the fresh catalyst samples in Fig. 2. These results indicate that the present catalysts are chemically and structurally stable to the total oxidation conditions probed (*vide infra*).

CO oxidation activity

Fig. 3 exhibits curves representing percentage of conversion (oxidation) of CO over the present catalysts as a function of reaction temperature. No products other than CO_2 were observed under the test conditions. In spite of the limits of this kind of representation of catalytic oxidation activity, as underlined by Hubbard *et al.*,[27] such data may facilitate revealing (*i*) the relative activity of a set of test catalysts, or (*ii*) changes

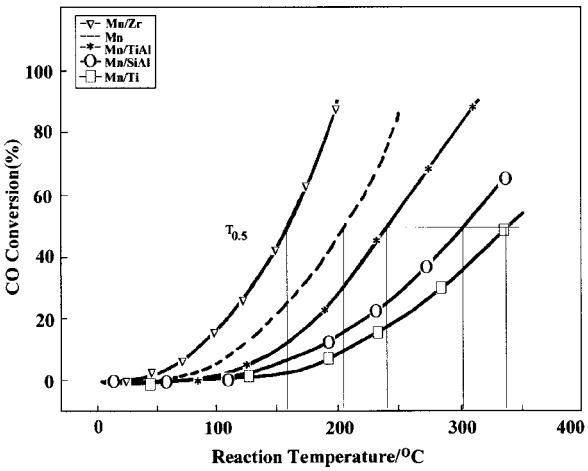

Fig. 3 Conversion of carbon monoxide as a function of temperature over the catalysts indicated ($T_{0.5}$ = temperature at which 50% conversion is achieved).

conceded by reaction mechanistic course. Adopting the temperature at which 50% conversion of CO is effected (denoted $T_{0.5}$) as activity criterion, in the sense that the higher the $T_{0.5}$ value the lower the activity, the present data make it obvious that on Zr ($T_{0.5}$ = 160 °C) the CO oxidation activity of Mn_2O_3 ($T_{0.5}$ = 210 °C) is detectably improved. In contrast the other supports show higher $T_{0.5}$: *viz.* 240, 305 and 340 °C for Mn/TiAl, Mn/SiAl and Mn/Ti, respectively. It should also be noted that the initial oxidation temperature, that is the temperature at which CO oxidation activity is triggered, occurs below 250 °C for all the catalysts. At such low temperatures, CO oxidation has been suggested[28,29] to follow a Eley–Rideal or Langmuir–Hinshelwood-type mechanism (*i.e.*, the oxidant is an adsorbed oxygen species). However, considering the $T_{0.5}$ values, the validity of such a suggestion appears to be confined only to Mn and Mn/Zr. On the other catalysts, $T_{0.5}$ assumes values ⩾250 °C, where catalytic oxidation of CO has been reported[28,30] to follow a Mars–van Krevelen-type mechanism (*i.e.*, the oxidant is lattice oxygen species).

Based on the fact that the unloaded supports showed no catalytic activity towards CO oxidation under the conditions applied, the above results are attributable to support-modified properties of Mn_2O_3. Consulting the data compiled in Table 1, Mn/Zr is found to be distinct by the coexistence on its surface of $Mn^{\leqslant 3+}$ sites. The other catalysts are found to expose $Mn^{\geqslant 3+}$ sites. Thus, it seems that d-d electron exchange interactions involving $Mn^{\geqslant 3+}$ sites are capable of creating the necessary electron-mobile environment[16] for surface redox reactions.[12]

Considering that the observed increase in the $T_{0.5}$ value (Fig. 3) arises from a change in the reaction mechanism towards a Mars–van Krevelen-type mechanism, one may expect generation of $Mn^{\leqslant 3+}$ sites on Mn/Ti, Mn/TiAl and Mn/SiAl to reinforce the following reported motivations: (*i*) suppression of O_2 chemisorption, or transformation of chemisorbed O_2 into less reactive surface species (*e.g.*, nucleophilic O^{2-} adsorbed species),[31] and/or weakening of the covalency of the metal-adsorbed oxygen bonds,[32] and (*ii*) enhancement of the mobility of lattice oxygen sites,[9] or weakening of the ionicity of metal-lattice oxygen bonds. Neglecting CO chemisorption is justified since the molecule is unlikely to adsorb on metal oxide surfaces above room temperature.[33]

CH_4 oxidation activity

Fig. 4 exhibits the percentage of conversion of CH_4 over the test catalyst as a function of reaction temperature. The conversion was due solely to total oxidation, and CO_2 and H_2O

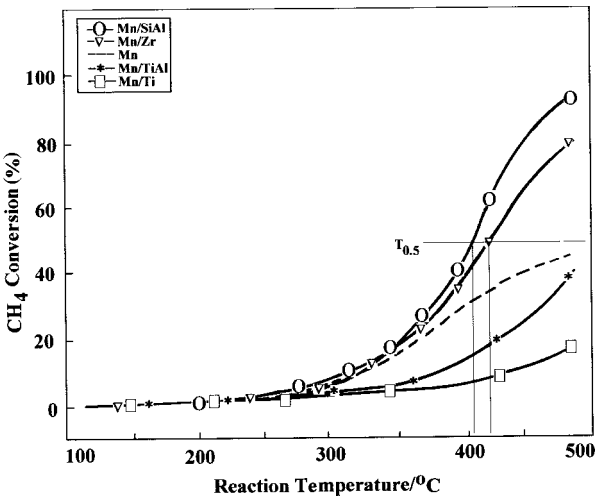

Fig. 4 Conversion of methane as a function of temperature over the catalysts indicated ($T_{0.5}$ = temperature at which 50% conversion is achieved).

were the final detectable products. In this reaction also, the unloaded supports exhibited no catalytic activity. Fig. 4 shows that CH_4 oxidation activity is developed for all catalysts at $\geqslant 250\,^{\circ}C$, and $T_{0.5}$ occurs at $>400\,^{\circ}C$. The trend of variation of the catalytic activity is largely similar to that shown (Fig. 3) towards CO oxidation, except for Mn/SiAl. The latter catalyst is shown to exhibit the highest activity towards CH_4 oxidation, whereas it occupies fourth place on the descending scale of activity towards CO oxidation.

The interaction of light hydrocarbons (including CH_4) with oxidized surfaces of $MgCr_2O_4$ (an active hydrocarbon combustion catalyst) has been investigated by *in situ* IR spectroscopy in the temperature range 25–500 °C.[5] It has been concluded that each hydrocarbon reacts at its weakest C–H bond with metal-oxygen sites giving rise, by hydrogen abstraction and C–O bond formation, to intermediate organic oxygenate surface species (alkoxy species and, then, carbonyl and/or carboxylate species), prior to eventual oxidative decomposition into CO_2 and H_2O. Because of the high activation temperatures required to oxidize CH_4 (the least active hydrocarbon),[5] only the latter surface intermediates (carboxylates or carbonate) were detectable. The authors[5] have reported that oxidation of CH_4 can be made easier on strongly acidic surfaces exposing metal sites of different oxidation states and active lattice O^{2-} sites (Mars–van Krevelen-type mechanism). Kinetic studies performed by Hu and Ruckenstein,[8] and by Stojanović *et al.*,[4] have agreed that CO is the primary oxidation product of CH_4 on metal oxide surfaces, and that CO_2 is only subsequently generated *via* further oxidation of CO. These authors have also agreed that the rate determining step is $C_s + O_s \rightarrow CO_s$, and that further oxidation of CO is much faster. Stojanović *et al.*[4] have proposed electron-mobilizing sites (*e.g.*, Ni–O–Ni ensembles) on $LaCr_{1-x}Ni_xO_3$ catalysts to be the key surface reagent.

Based on the above literature background, the observed similarity of support effects of zirconia, titania and titania–alumina on the catalytic activity of Mn_2O_3 towards oxidation of CO (Fig. 3) and CH_4 (Fig. 4) is expected. This is consistent with a higher rate of oxidation of CO (primary oxidation product of CH_4), for a higher overall rate of total oxidation of CH_4 into CO_2 (and H_2O). The odd behaviour of Mn/SiAl, being less active in CO oxidation, but most active in CH_4 oxidation, may be related, according to Finocchio *et al.*,[5] to the relatively stronger acidity of the silica–alumina support.[21] Generally speaking, however, the present supported Mn_2O_3 catalyst, particularly on silica–alumina and zirconia, exhibits comparable CH_4 combustion activity to that of the most active hydrocarbon combustion catalysts of spinel[1,5] and perovskite[1–3] structured oxides. This fact, together with the observed chemical and structural stabilities of supported Mn_2O_3 under the reaction conditions, may make it a promising practical combustion catalyst.

Conclusion

The above presented and discussed results indicate that unsupported MnO_x species (exposed on an α-Mn_2O_3 bulk structure) catalyze total oxidation of both CO and CH_4, without being altered, either chemically or structurally, under the reaction conditions. They demonstrate, however, that no apparent relation exists between the CO and CH_4 oxidation activities, though CO is a known oxidation intermediate for CH_4. Occurrence of the oxidation of CH_4 at a much higher temperature regime ($\geqslant 250\,^{\circ}C$) than that ($\leqslant 250\,^{\circ}C$) in which CO oxidizes, may imply that CO oxidation is not the rate determining step. The fact that the CO oxidation activity is improved when MnO_x is supported on zirconia, whereas CH_4 oxidation is improved further when silica–alumina is used as support material, may indicate that different catalytic functions are implicated in the rate determining step. Indeed, C–H activation, known to be rate determining for CH_4 oxidation, would be favoured on a strongly acidic surface such as that of silica–alumina. Thus, the difference in the catalytic activity towards the oxidation of CO and CH_4 resides in the need for different catalytic functions for each reaction, which are therefore not related in terms of kinetic control. The XPS-raised question about the actual oxidation state of Mn that drives the activity for CO oxidation on the various catalysts, may sustain such reasoning.

Acknowledgements

The financial support of Kuwait University (Research Administration Grants No. SC076 and SC095) and the excellent technical support of the general research facilities (Analab/SAF) of the Faculty of Science are highly appreciated. N.E.F. thanks the Alexander von Humboldt Foundation for a grant, whereby such a fruitful collaboration between Kuwait and Munich Universities was facilitated.

References

1 R. L. Garten, R. A. Dalla Betta and J. C. Schlatter, in *Handbook of Heterogeneous Catalysis*, eds. G. Ertl, H. Knözinger and J. Weitkamp, Wiley-VCH, Weinheim, 1997, vol. 4, pp. 1668–1677.
2 L. Marchetti and L. Forni, *Appl. Catal. B*, 1998, **15**, 179.
3 G. Saracco, G. Scibilia, A. Iannibello and G. Baldi, *Appl. Catal. B2*, 1996, **8**, 229.
4 M. Stojanović, C. A. Mims, H. Houdallal, Y. L. Yang and A. J. Jacobson, *J. Catal.*, 1997, **166**, 324.
5 E. Finocchio, G. Busca, V. Lorenzelli and R. J. Willey, *J. Catal.*, 1995, **151**, 204.
6 M. Zwinkels, S. G. Jaras and P. G. Menon, *Catal. Rev., Sci. Eng.*, 1993, **35**, 261.
7 A. Cybulksi and J. Moulijin, *Catal. Rev., Sci. Eng.*, 1994, **36**, 179.
8 Y. H. Hu and E. Ruckenstein, *J. Catal.*, 1996, **158**, 260.
9 P. J. Gellings and H. J. M. Bouwmeester, *Catal. Today*, 1992, **12**, 1.
10 D. Dissanayake, J. H. Lunsford and M. P. Rosynek, *J. Catal.*, 1993, **143**, 286.
11 V. A. Matyshak and O. V. Krylov, *Catal. Today*, 1995, **25**, 1.
12 M. I. Zaki, M. A. Hasan, L. Pasupulety and K. Kumari, *New J. Chem.*, 1998, **22**, 875.
13 T. Seiyama, *Catal. Rev., Sci. Eng.*, 1992, **34**, 281.
14 P. E. Marti and A. Baiker, *Catal. Lett.*, 1994, **26**, 71.
15 M. I. Zaki, A. K. H. Nohman, C. Kappenstein and T. M. Wahdan, *J. Mater. Chem.*, 1995, **5**, 1081.
16 C. Zener, *Phys. Rev.*, 1951, **81**, 440; *ibid.*, 1951, **82**, 403; *ibid.*, 1951, **83**, 299; *ibid.*, 1952, **85**, 324.

17 B. Delmon, in *Handbook of Heterogeneous Catalysis*, eds. G. Ertl, H. Knözinger and J. Weitkamp, Wiley-VCH, Weinheim, 1997, vol. 1, pp. 264–283.
18 G.-M. Schwab and E. Schwab–Agallidis, *Ber. Dtsch. Chem. Ges.*, 1943, **76**, 1228; G.-M. Schwab and G. Holz, *Z. Anorg. Chem.*, 1944, **252**, 205; G.-M. Schwab and A. Karatzas, *Z. Elektrochem.*, 1944, **50**, 242.
19 R. J. Matyi, L. H. Schwartz and J. B. Butt, *Catal. Rev., Sci. Eng.*, 1987, **29**, 41.
20 W. B. White and V. G. Keramidas, *Spectrochim. Acta, Part A*, 1972, **28**, 501.
21 A. Iordan, C. Kappenstein, E. Colnay and M. I. Zaki, *J. Chem. Soc., Faraday Trans.*, 1998, **94**, 1149.
22 M. Che and L. Bonneviot, *Pure Appl. Chem.*, 1987, **27**, 1.
23 G. A. Parks, *Chem. Rev.*, 1965, **65**, 177.
24 G. D. Parfitt, *Pure Appl. Chem.*, 1976, **48**, 415.
25 J. P. Brunelle, *Pure Appl. Chem.*, 1978, **50**, 1211.
26 M. I. Zaki and C. Kappenstein, *Z. Phys. Chem.* (*Munich*), 1992, **176**, 97.
27 C. P. Hubbard, K. Otto, H. S. Gandhi and K. Y. S. Ng, *J. Catal.*, 1993, **144**, 484.
28 A. Bielański and J. Haber, *Oxygen in Catalysis*, Marcel Dekker Inc., New York, 1991, pp. 211–271.
29 H. Kung, *J. Catal.*, 1982, **73**, 387.
30 E. S. J. Lox and B. H. Engler, in *Handbook of Heterogeneous Catalysis*, eds. G. Ertl, H. Knözinger and J. Weitkamp, Wiley-VCH, Weinheim, 1997, vol. 4, pp. 1595–1633.
31 M. Che and A. J. Tench, *Adv. Catal.*, 1982, **31**, 77; *ibid.*, 1983, **32**, 1.
32 H. Kung and M. Kung, *Adv. Catal.*, 1984, **33**, 159.
33 M. I. Zaki and H. Knözinger, *Spectrochim. Acta, Part A*, 1987, **43**, 1455; *Mater. Chem. Phys.*, 1987, **17**, 201.

Paper 9/07468F